mathematics

MDPI

Article

Controlling Effects of Astrocyte on Neuron Behavior in Tripartite Synapse Using VHDL–AMS

Osman Taylan [1], Mona Abusurrah [2], Ehsan Eftekhari-Zadeh [3,*], Ehsan Nazemi [4], Farheen Bano [1] and Ali Roshani [5]

1 Department of Industrial Engineering, Faculty of Engineering, King Abdulaziz University, P.O. Box 80204, Jeddah 21589, Saudi Arabia; otaylan@kau.edu.sa (O.T.); fbano@kau.edu.sa (F.B.)
2 Department of Management and Information Systems, College of Business Administration, Taibah University, Medina 42353, Saudi Arabia; mabusurrah@taibahu.edu.sa
3 Institute of Optics and Quantum Electronics, Friedrich Schiller University Jena, Max-Wien-Platz 1, 07743 Jena, Germany
4 Imec-Vision Lab, Department of Physics, University of Antwerp, 2610 Antwerp, Belgium; ehsan.nazemi@uantwerpen.be
5 Computer Engineering Department, Kermanshah University of Technology, Kermanshah 6715685420, Iran; aliroshani@kut.ac.ir
* Correspondence: e.eftekharizadeh@uni-jena.de

Abstract: Astrocyte cells form the largest cell population in the brain and can influence neuron behavior. These cells provide appropriate feedback control in regulating neuronal activities in the Central Nervous System (CNS). This paper presents a set of equations as a model to describe the interactions between neurons and astrocyte. A VHDL–AMS-based tripartite synapse model that includes a pre-synaptic neuron, the synaptic terminal, a post-synaptic neuron, and an astrocyte cell is presented. In this model, the astrocyte acts as a controller module for neurons and can regulates the spiking activity of them. Simulation results show that by regulating the coupling coefficients of astrocytes, spiking frequency of neurons can be reduced and the activity of neuronal cells is modulated.

Keywords: neuron; astrocyte; tripartite synapse

Citation: Taylan, O.; Abusurrah, M.; Eftekhari-Zadeh, E.; Nazemi, E.; Bano, F.; Roshani, A. Controlling Effects of Astrocyte on Neuron Behavior in Tripartite Synapse Using VHDL–AMS. *Mathematics* **2021**, *9*, 2700. https://doi.org/10.3390/math9212700

Academic Editor: Ilya V. Sysoev

Received: 10 September 2021
Accepted: 20 October 2021
Published: 25 October 2021

1. Introduction

Several different computational approaches, such as Runge–Kutta methods, finite element, numerical linear algebra, statistics, numerical analysis, tensor analysis, and the most important one, Neural Networks (NNs), have been used in various fields of researches such as chemical engineering [1–9], electrical engineering [10–19], health and biology [20–34], fluid mechanic engineering [35–46], civil engineering [47–50], computer sciences [51–53], petroleum engineering [54–62], and mathematics [63–74] etc. The most important and most applicable method is NNs, which has been inspired by human neural networks. Every attempt to understand the natural neural network and modeling its structure can lead to powerful tools for solving the above-mentioned engineering problems.

Scientific reports about the topology of the output patterns in biological neural networks show that neurobiology is now finding new ways to explain the different states of data processing in the human brain [75]. To achieve a comprehensive view of the CNS, a compact biological system by a large number of building blocks, neurons, and synapses can be considered [76]. According to recent research, the description of the CNS in the absence of astrocytes is not perfect, and to attain a comprehensive system operation model, astrocyte cells' properties must be considered [77]. In the human brain, neurons, which form the basic building blocks, are in a close relationship with astrocyte cells. Astrocyte cells could be of importance in terms of information and data processing in the brain. It has been illustrated that astrocytes have a bidirectional interaction with neuronal cells,

which has vital effects on various biological conditions. In addition, these cells are subtypes of glial cells in the CNS and capable of supporting different metabolic features [78]. Astrocytes, which are inactive cells in terms of excitability and active voltage, release calcium ions in the brain. A large number of scientific reports illustrate the vital role of astrocytes in protecting and controlling neurons [79]. Therefore, investigation of the neuron–astrocyte interaction effects is very significant in biology [80]. In this approach, neural–glial modeling and different aspects of their interaction can help to detect various biological states of the CNS [77]. These astrocyte cells can have several functional roles, such as extracellular environment regulation, synaptic information regulation, neuronal synchronization, and feedback to neural activity [75,77,81]. One of the most important roles of astrocytes is their controlling effect on neurons. Based on tue tripartite synapse model, neurons can stimulates the astrocyte via pathways, and astrocytes also produce the stimulation current of neuronal cells [77,82]. Therefore, astrocytes have a basic role in providing input stimulation of neurons, and by suitable parameter choices, the applied stimulation can be reduced. Consequently, spiking behaviors are regulated. In this way, we can use the VHDL–AMS process, which is very useful and simple for modeling the systems. This paper presents mechanisms of astrocytes' effects on neurons using VHDL–AMS. In this paper, we consider the neuron–astrocyte interaction model by VHDL–AMS for evaluating all activation pathways that help us select the suitable coefficient parameters. In the mathematical model of neuron–astrocyte interaction, there are some nonlinear terms, and their implementations need some approximations. In fact, because of the non-linearity of the mathematical equations that describe the biological systems, some approximations are required for realizing these systems. On the other hand, to implement the neuronal models, we must consider some linear and modified models that mimic the original models with high precision and low errors. In these approaches, some papers have focused on the VHDL digital implementations of the neuronal models [75,76,83–88]. In these papers, neuronal models have been modified based on the mathematical approximations and were eventually realized on digital platforms such as FPGA. This procedure needs some modifications and may be timely. Consequently, the VHDL–AMS method is very suitable choice for evaluating the systems. Since this approach is capable of behavioral modeling, linear and nonlinear systems are close together in the case of operation [89,90]. In this way, to achieve a useful and simple modeling of neuron–astrocyte interaction, VHDL–AMS stands out due to its convenience as a suitable option [89,90]. Furthermore, the digital and analog sections of the system are coupled in this procedure. In this paper, our strategy is to realize the different processes of neuron–astrocyte interaction leading to controlling effects using VHDL–AMS. In other words, by modeling the neuron–astrocyte interaction model, different effects of the astrocyte module on the neurons activity will be evaluated.

The rest of this paper is as follows: Interaction between neuronal and glial cells is described in Section 2. Tripartite synapse is described in Section 3. Section 4 presents a model based on the tripartite synapse. Section 5 presents the controlling effect for astrocyte. Simulation results are given in Section 6. A brief discussion is presented in Section 7. The paper concludes in Section 8.

2. Neural–Glial Interaction

Astrocytes are important components of the neurobiological communication system, and they have the ability to modulate neuronal activity. Glutamate is released into the synaptic gap when neurons fire, and it is partially attached to the astrocytes' metabotrobic glutamate receptors (mGluR). G-protein-coupled glutamate receptors, which regulate a number of intercellular signaling pathways, are known as metabotrobic glutamate receptors. Group-I glutamate receptors are a subtype of metabotrobic glutamate receptors that are linked to polyphosphoinositol hydrolysis. Inositol 1,4,5-triphosphate (IP3), a type of polyphosphoinoside, which works as a second messenger and modulates calcium signaling, is a critical participant in the release of calcium from internal storage. When glutamate binds to the astrocyte, IP3 is released into the astrocyte's intracellular space. Ca is released

from the ER into the cytosol after IP3 interacts with the IP3 receptor in the endoplasmic reticulum (ER). On the other hand, the level of inositol 1,4,5-triphosphate is controlled by external signals that reach the cell. The release of glutamate from the astrocyte is triggered by an increase in intracellular calcium levels in astrocytes, which is augmented by extracellular glutamate, modifying the pre-synaptic and post-synaptic depolarizing currents in neurons. Furthermore, nonlinear amplitude and frequency modulation events represent inositol 1,4,5-triphosphate dynamics, whereas calcium oscillations are fundamentally frequency-modulated [91]. To describe the architecture of the mathematical modeling, which is explained in the next parts, Figure 1 depicts all important pathways of the system. In this case, several important mediators are considered to cause increases in the intercellular $[K^+]$, triggering the removal of potassium by glions, etc. In this structure, two activation pathways for the glia can be evaluated: fast and slow mechanisms. The fast process is shown by the glion depolarization in case of rise of the extracellular potassium concentration. Furthermore, the slow process is considered by the IP3 production initiated by synapse mediator diffusion. Moreover, a different pathway is applied for the glial response both to the pre-synaptic neuron (its synaptic terminal) and to the post-synaptic neuron [77,82,92,93].

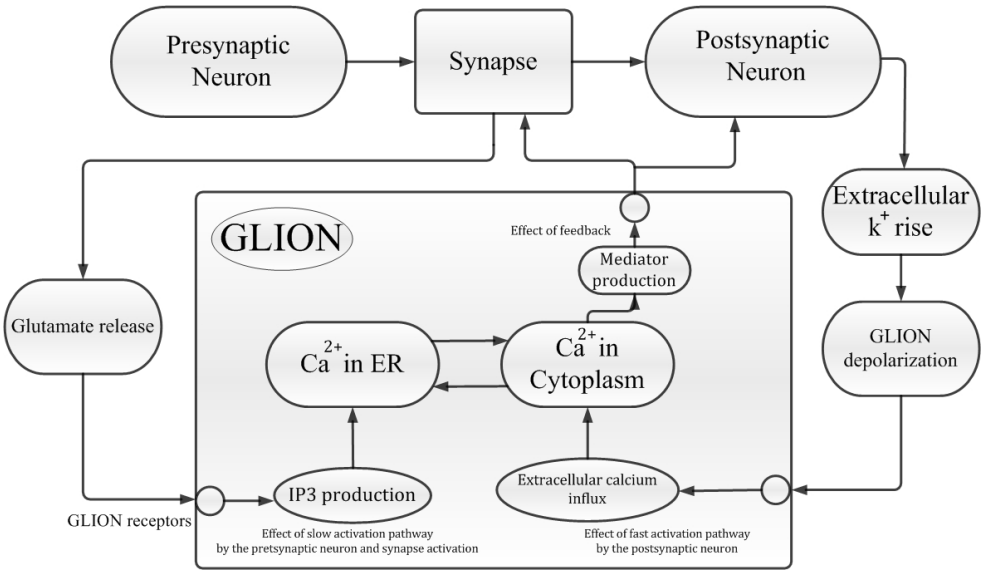

Figure 1. Functional structure of neural–glial interaction.

3. Tripartite Synapse

As depicted in Figure 2, the basic tripartite synapse consists of a synapse gap that can connect a pre-synaptic neuronal cell to a post-synaptic neuronal one. In this network, an astrocyte cell is in a bidirectioal connection with them [77].

In this system, oscillatory behavior in an astrocyte cell can be produced by two main pathways: the fast and the slow pathways. The fast activation pathway can be activated by the post-synaptic neuron. Consequently, astrocyte cells reproduce the calcium waves as an external oscillation.

The slow activation pathway can be considered by the pre-synaptic neuron-spiking behaviors. In this way, by triggering the synapse with a pre-neuron, astrocyte will be stimulated. After this stimulation, astrocyte generates the secondary mediator (S_m) in the intra area. Therefore, it can trigger the calcium release and then creates calcium oscillations.

A feedback mechanism is observable by the astrocyte mediator (G_m), which can influence both the synapse gap and the post-neuron behavior simultaneously. Thus, by producing calcium oscillations in the astrocyte, the mediator enters the internal area, and the regulation of neurons activity will be achieved.

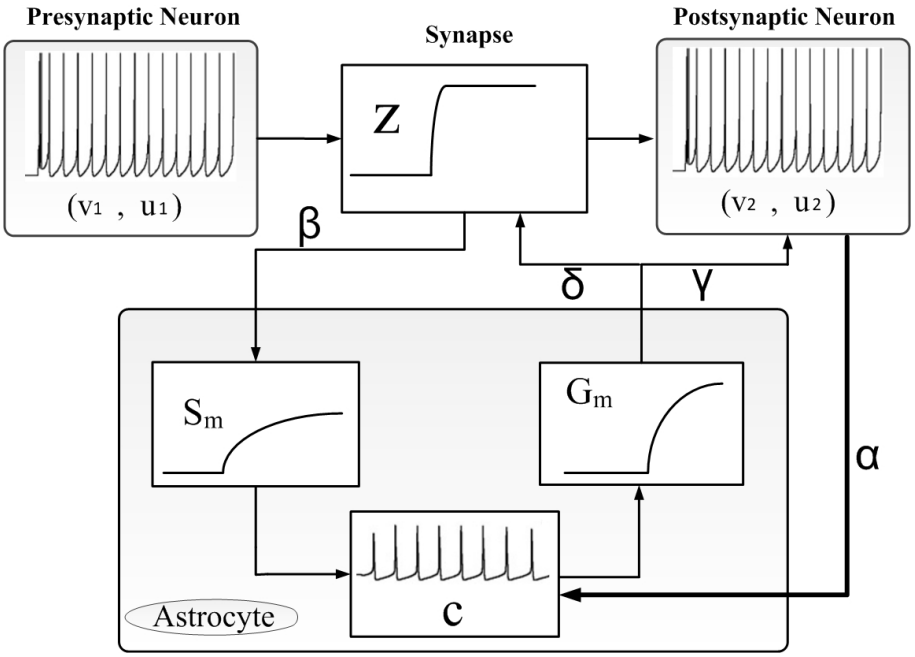

Figure 2. Mechanisms of interaction between neurons and astrocyte in the tripartite synapse based on coupling coefficients, $\alpha, \beta, \gamma, \delta$.

4. System Modeling Using VHDL–AMS

The VHDL–AMS technique help us to reduce the simulation and realization time of the system modeling. Thus, this approach can be a very useful case to evaluate and process the complex systems without any mathematical approximations or estimations [89,90]. In addition, VHDL–AMS behavioral modeling of the systems can be handled so that we can have a real dynamical system. On the other hand, since the basic elements of the biological systems have the nonlinear parts, it is expected to need a total approximation of them to be implemented. This procedure can require a long time sequence. Therefore, by using the VHDL–AMS for modeling these nonlinear and complex mathematical equations, the exact and real results are observable, similar to a real hardware. The VHDL–AMS modeling of neuron-astrocyte interaction has been done as follows.

We have modeled the behavior of this interaction as a compact system that connects two coupled neurons together, and an astrocyte cell controls the coupling behaviors of them. Different parameters of the astrocyte can influence the behaviors of neuronal signals. Each parameter in this system can influence the frequency and time of spiking in the pre-synaptic and post-synaptic neurons. Consequently, by proper selection of the astrocytic parameters, the spiking behaviors of the neuronal cells will be modulated.

4.1. Neuron and Synapse Modeling

The Izhikevich neuron model gives the recognized behavior of neuron dynamics, where different spiking and bursting signals are shown. Another advantage is that the model has real-time properties. The Izhikevich neuron model can reproduce all of the 20 firing schemes. On the other hand, this neuron model is capable of reproducing many different firing behaviors that can occur in biological spiking neurons. To explain the pre- and post-neuronal cells, the Izhikevich neuronal model is considered [94], which consists of two coupled differential equations:

$$\frac{dv}{dt} = 0.04v^2 + 5v + 140 - u + I \tag{1}$$

$$\frac{du}{dt} = a(bv - u) \tag{2}$$

By conditional reset equations:

$$if \quad v > v_{th} \qquad then \quad \begin{cases} v \longleftarrow c \\ u \longleftarrow u + d \end{cases} \tag{3}$$

Here, v denotes the voltage variable and u represents a recovery variable, which accounts for the activation of K^+ ionic currents and inactivation of Na^+ ionic currents, and it provides negative feedback to v. In these equations, I is the input stimulation of neurons. In the pre-neuronal equation, $I_{Presynaptic} = I_{stimulate}$ is the input stimulus such that that, by this excitation, the tripartite synapse can be triggered and generates a set of spikes. If the synaptic gap triggers the pre-neuron, the stimulus current of the synapse $I_{Synapse}$ is genereted, and the astrocyte cell also generates its stimulus current, $I_{Astrocyte}$. Consequently, the excitation of post-synaptic neuron is produced by two different ways:

$$I_{Postsynaptic} = (K_{Modified})I_{Synapse} + I_{Astrocyte} \tag{4}$$

where

$$I_{Synapse} = (k_s - \delta G_m)(z - z_0) \tag{5}$$

$$I_{Astrocyte} = \gamma G_m \tag{6}$$

$$K_{Modified} = 0.01 \tag{7}$$

In these equations, γ and δ control the astrocytic and synaptic currents, respectively, in the case of regulating the post-synaptic neurons activity.

Moreover, in this model, the synapse terminal is capable of connecting a pre-synaptic neuron to a post-synaptic one and can be modeled as follows [88,95]:

$$\tau_s \frac{dz}{dt} = [1 + \tanh(S_s(v_1 - h_s))](1 - z) - \frac{z}{d_s} \tag{8}$$

Here, z is a variable for synaptic activation, and other parameters of synapse are also given as

- τ_s : delay (s) ;
- S_s, d_s : activation and relaxation of z ;
- h_s : Threshold parameter ;
- $I_{Synapse}$: Synapse stimulus current ;
- k_s : Conductance ;
- δG_m : Response for astrocyte ;
- z_0 : Reference state of z .

z_0 is the initial state of synaptic activation variable.

By triggering synapse with the pre-synaptic neuron, if $v_1 < h_s$, the synapse is inactive and $z = 0$. Increasing v_1 makes the hyperbolic tangent function differ with a high value and $z = 1$ with the rate of $1/\tau_s$. By activation of the synapse terminal, the voltage of pre-synaptic neuron is transferred to the post neuron.

4.2. Astrocytic Cell

In the CNS, the tripartite synapse [77,82] explains how two coupling neurons are connected to each other in a general formation. As depicted in Figure 2, the astrocyte module produces two main mediators: the secondary mediator (S_m) and the glia mediator (G_m). Moreover, calcium dynamics in the astrocyte is represented by c. Mathematical modeling is given by

$$\tau_c \frac{dc}{dt} = -c - c_4 f(c, c_e) + (r + \alpha u_2 + \beta S_m) \tag{9}$$

$$\varepsilon_c \tau_c \frac{dc_e}{dt} = f(c, c_e) \tag{10}$$

$$f(c, c_e) = c_1 \frac{c^2}{1+c^2} - \left(\frac{c_e^2}{1+c_e^2}\right)\left(\frac{c^4}{c_2^4+c^4}\right) - c_3 c_e \tag{11}$$

$$\tau_{S_m} \frac{dS_m}{dt} = [1 + \tanh(s_{Sm}(z - h_{S_m}))](1 - S_m) - \frac{S_m}{d_{S_m}} \tag{12}$$

$$\tau_{G_m} \frac{dG_m}{dt} = [1 + \tanh(s_{G_m}(c - h_{G_m}))](1 - G_m) - \frac{G_m}{d_{G_m}} \tag{13}$$

In these equations, the variable c denotes the cytoplasmic calcium, and c_e is responsible for the calcium in the endoplasmic reticulum. The excitation part, $(r + \alpha u_2 + \beta S_m)$ shows the external effects of different pathways on the astrocyte. Furthermore, $f(c, c_e)$ describes the relationship between cytoplasmic and ER calcium oscillations. Moreover, by the triggering of the synapse (z), IP3 (S_m) will be evoked, and by the production of calcium (c), the glutamate (G_m) will be released. Furthermore, as depicted in Figure 2, different pathological states of the neural–glial interaction can be evaluated by different parameters such as α, β, γ, and δ. In other words, by variation of these vital parameters, different interaction behaviors are generated. Different parameters of the CNS modeling are given in Table 1.

Table 1. Different Parameters of the CNS Modeling.

$c_1 = 0.13$	$c_2 = 0.9$	$c_3 = 0.004$	$c_4 = 50$	$\varepsilon_c = 0.04$
$\tau_c = 8$	$\tau_{S_m} = 100$	$\tau_{G_m} = 50$	$s_{S_m} = 100$	$s_{G_m} = 100$
$h_{S_m} = 0.45$	$h_{G_m} = 0.5$	$d_{S_m} = 3$	$d_{G_m} = 3$	$S_s = 1$
$h_s = -68$	$d_s = 3$	$\tau_s = 10$	$k_s = 1000$	$z_0 = 0.0002$
$a = 0.02$	$b = 0.2$	$c = -65$	$d = 6$	$I_{Stimulation} = 14$

5. Controlling Effects of Astrocyte Module

The oscillatory behaviors of active neurons in the brain are very important issue in terms of unstable conditions, which may be causes different problems such as high rate of oscillations between pre- and post-neuronal cells. This additional oscillatory and high-rate activity synchronized neurons in ranges of times, and some problems may occurs such as epilepsy in the case of synchronized additional spiking activity [88,96,97]. In this approach, the astrocyte biological cell plays a vital and significant role in adjusting the neuronal behaviors in terms of controlling effects on them in the CNS. Furthermore, astrocyte cells generate the excitation currents for the post-neurons at different levels. Since the applied stimulus current of post-synaptic neuron depends on the synaptic transmission and astrocyte activity, the appropriate selection of feedback coefficients, γ and δ, is very important. As can be seen in Figure 3 and also Equations (4)–(6), the excitation current of the post-neuron can be reduced by the effect of astrocytic cells on the synapse transmission that is proportional to δ. This excitation current can be increased by the direct effect of astrocyte cell on the post-neuronal cell, which is proportional to γ. Therefore, if the coupling coefficients, γ and δ are not adjusted, the input excitation current of the post-neuron can be significantly increased, and the frequency of the spiking behavior is increased. However, if γ is reduced and δ is increased, spiking behavior of the post-neuron by decreasing input current can be regulated.

From mathematical point of view, the stimulation of the post-neuron can be rewritten as

$$I_{Postsynaptic} = K_{Modified} K_s Z + (\gamma - K_{Modified} \delta Z) G_m \tag{14}$$

Based on this stimulation of post-synaptic neuron, the role of γ, δ as a control parameters of astrocytes are very important.

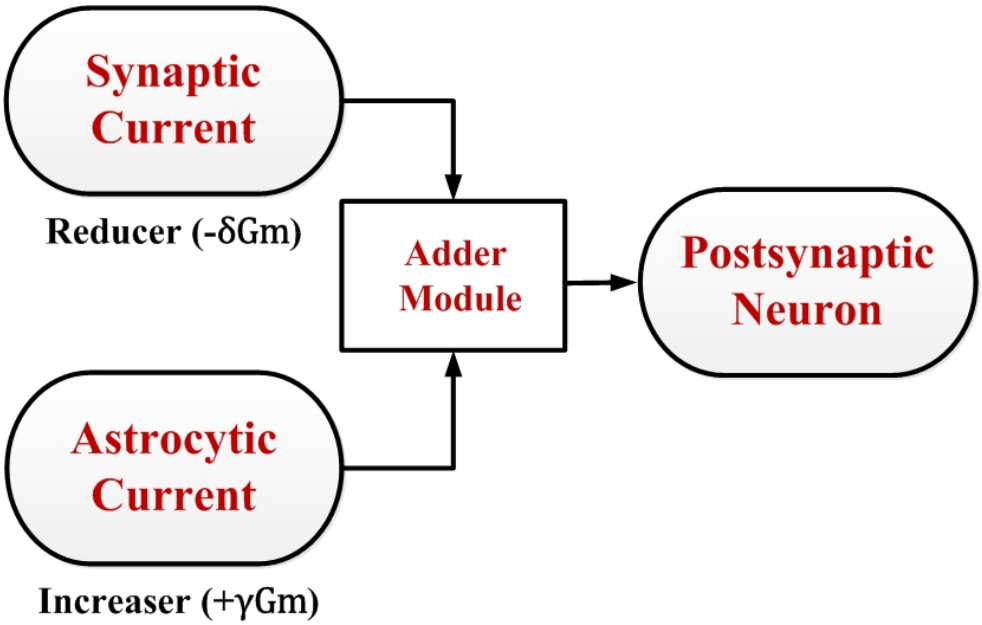

Figure 3. Input excitation current of post-synaptic neuron that is created by the synapse and astrocyte at the same time.

6. Simulation Results

The results of neuron–astrocyte interaction simulation with VHDL–AMS are given in this part. In this way, different effects of astrocyte parameters on the neurons behavior are evaluated.

This section presents the results of the simulation of the impact of astrocytes on the post-synaptic neuron behavior in the general case. In all cases, it assumed that the fast activation pathway is blocked and the slow activation pathway for the feedback activity is selected.

In the first case, we assume that $\delta = 0$, such that the effect of reduction coefficient in the post-synaptic neuron current is removed. In this state, we assume that $z_0 = 0$ and the excitation of the post-neuronal cell is given as

$$I_{Postsynaptic} = K_{Modified} K_s Z + \gamma G_m \tag{15}$$

Thus, based on the Equation (15), due to a high value of γ, the post-neuron excitation current will be significantly increased and cause adverse effects on neuronal activity. Furthermore, In Figures 4–6, the time interval of the post-synaptic neuron activity for different amounts of γ and δ is represented. As depicted in these figures, with increasing γ, the time interval for the post-neuron activity is increased, and with increasing δ, this problem can be solved. On the other hand, as δ is increased and γ is decreased, the spiking activity of post-synaptic neuron can be regulated.

Also, as depicted in Figure 7, simulation results for this case based on different values of γ are presented. When $\gamma = 0$, pre- and post-neuronal cells are simultaneously found in the spiking activity. By increasing γ, we can see that the post-synaptic neuron activity at some point in time is independent of the pre-synaptic neuron activity. Thus, if the feedback coefficient of the astrocyte increases strongly, the spiking frequency will also be increased.

In the second case, we assume that $\gamma = 0$, such that the effect of incremental coefficient in the post-synaptic neuron current is removed. Thus, the input excitation of post-synaptic neuron is given as

$$I_{Postsynaptic} = K_{Modified}(K_s - \delta G_m)Z \tag{16}$$

Based on this equation, δ controls the input current of the post-synaptic neuron, and since $\gamma = 0$, the post-synaptic neuron is starts to spiking activity in the time interval of the pre-synaptic neuron and not an independent activity.

As depicted in Figure 8 at $\delta = 0$, both the pre-synaptic and post-synaptic neurons are simultaneously activated. By increasing δ, the intensity of post-synaptic neuronal cell activity will be reduced.

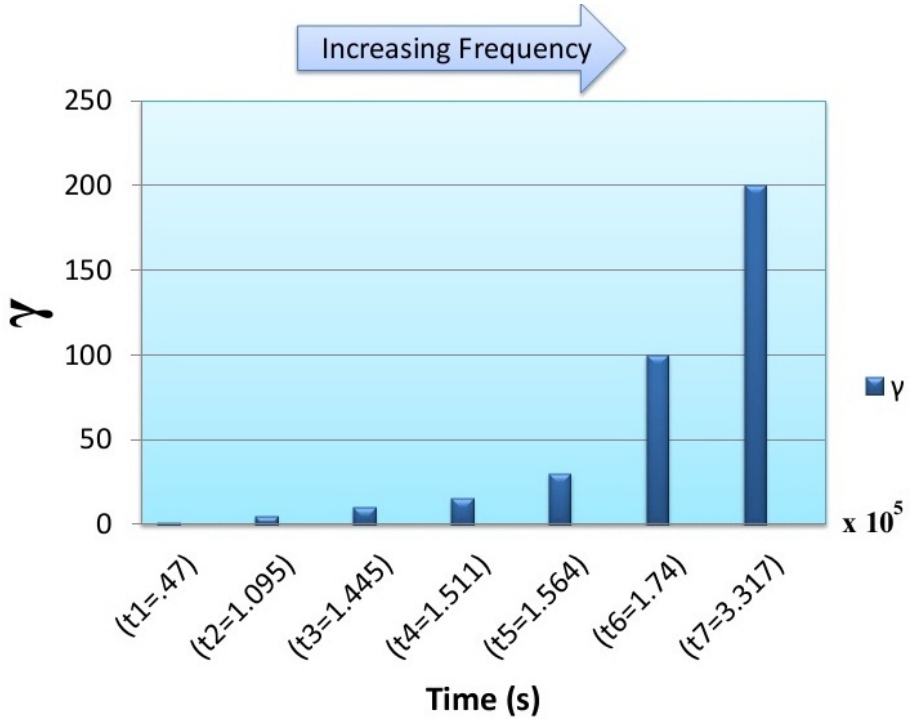

Figure 4. Effect of feedback coupling coefficient γ on the frequency and spiking interval of post-synaptic neuron.

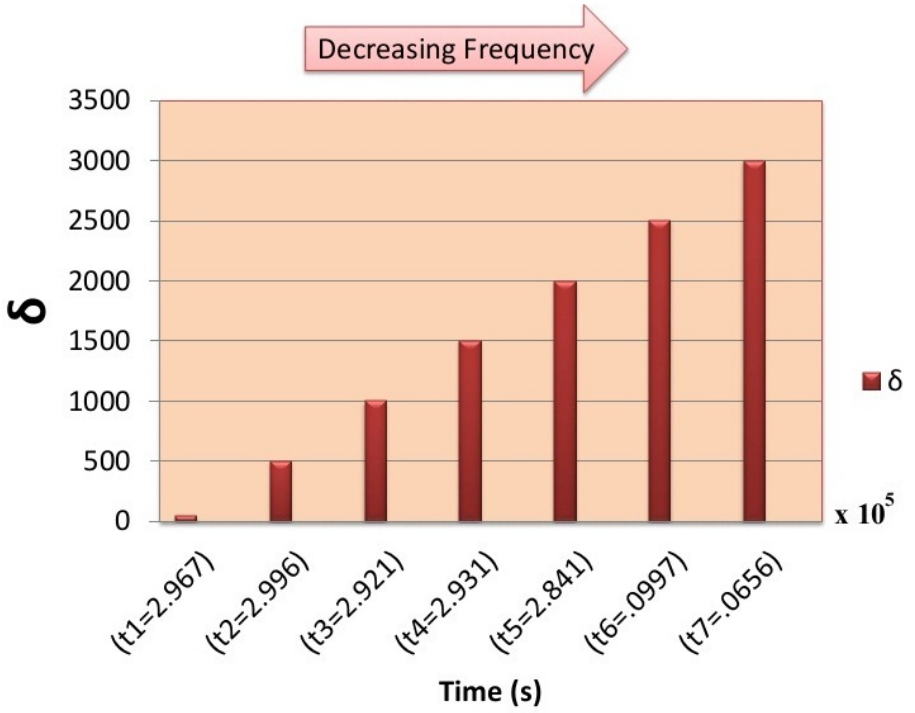

Figure 5. Effect of feedback coupling coefficient δ on the frequency and spiking interval of post-synaptic neuron.

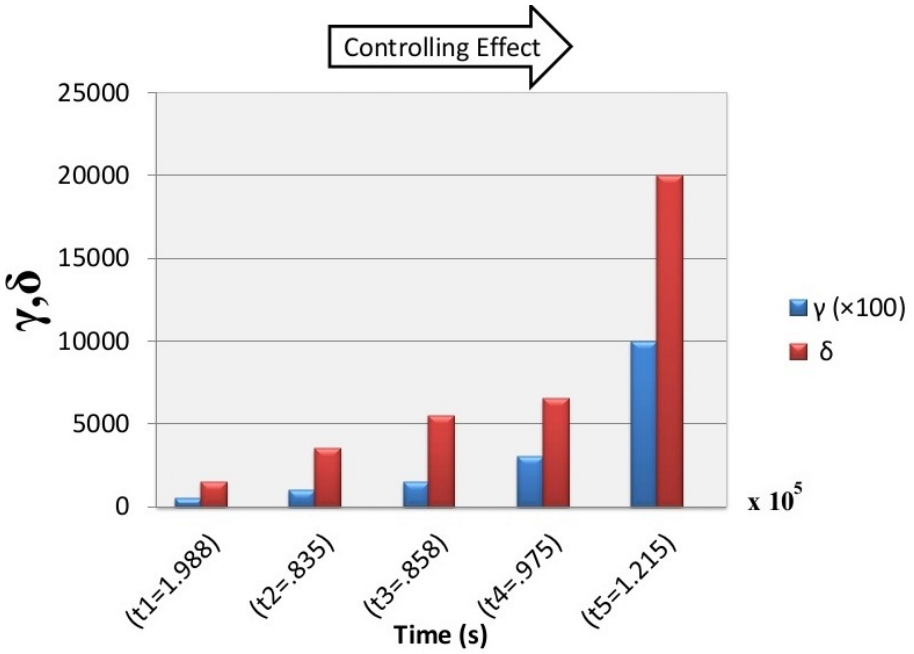

Figure 6. Effect of γ and δ at the same time. Spiking activity of post-synaptic neuron can be modulated.

In the third state, two parameters γ and δ influence spiking behaviors. In this state, as δ increases, the effect of γ in the subscribe time interval will be neutralized. In this case, based on the γ parameter, the post-synaptic neuron starts to activate, again by interruption in the pre-neuron activity. Different states for this case are shown in Figure 9.

It is illustrated that astrocytes are able to control the synaptic coupling behaviors by proper selection of parameters. In this way, the feedback behavior in the neural–glial interaction will be regulated and can prevent problems in neural networks.

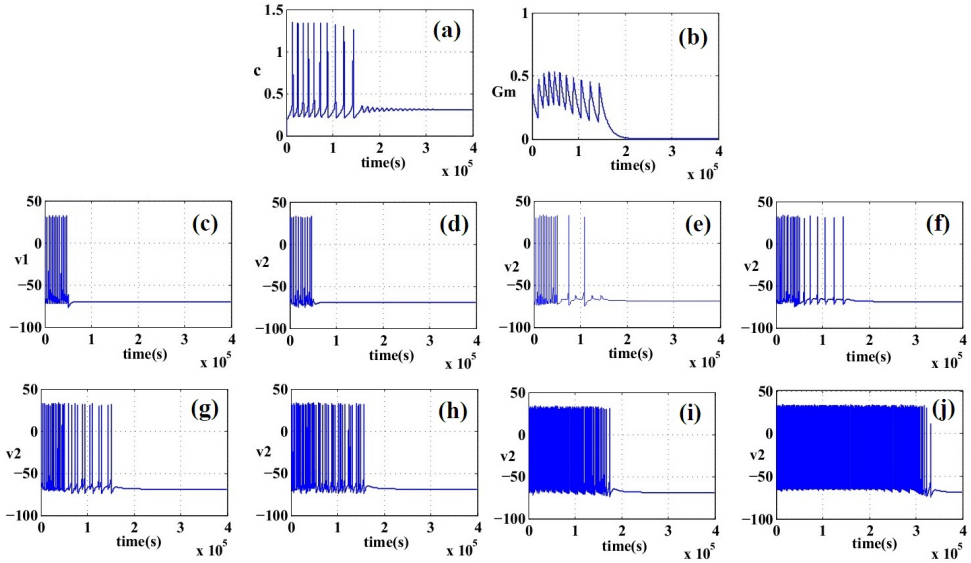

Figure 7. Closed-loop behavior in the neural glial interaction. (**a**) Calcium dynamic. (**b**) Astrocyte mediator (glutamate). (**c**) Spiking activity of pre-synaptic neuron. (**d**–**j**) Spiking activity of post-synaptic neuron based on different values of γ. By increasing γ, the intensity of neural activity has been increased.

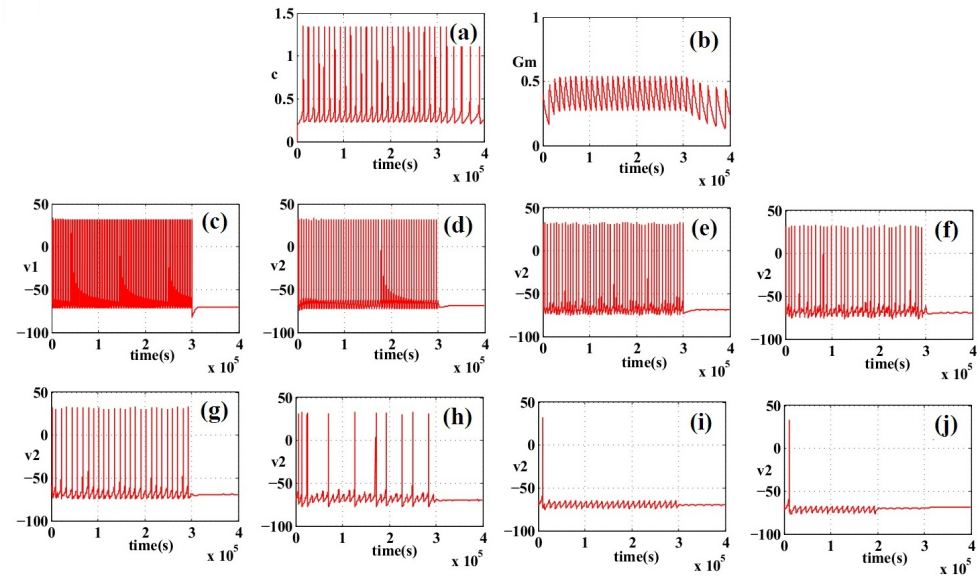

Figure 8. Closed-loop behaviour in the neural–glial interaction. (**a**) Calcium dynamic. (**b**) Astrocyte mediator (glutamate). (**c**) Spiking activity of pre-synaptic neuron. (**d**–**j**) Spiking activity of post-synaptic neuron based on different values of δ. By increasing δ, the intensity of neural activity is decreased and the spiking activity is controlled.

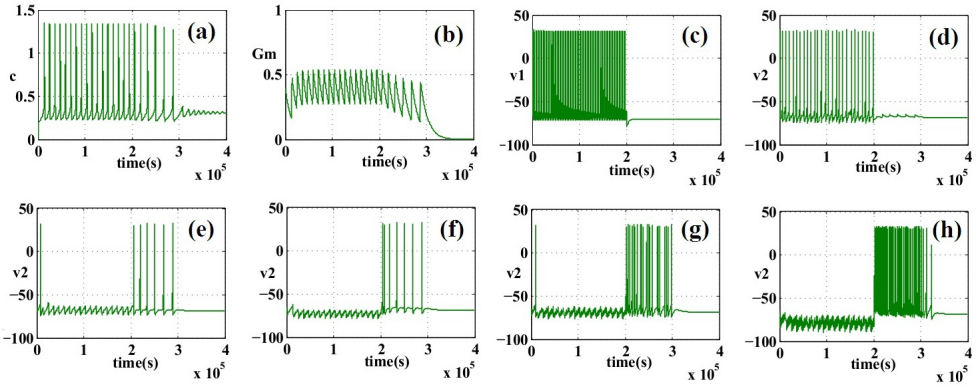

Figure 9. Closed-loop behavior in the neural–glial interaction. (**a**) Calcium dynamic. (**b**) Astrocyte mediator (glutamate). (**c**) Spiking activity of pre-synaptic neuron. (**d**–**h**) Spiking activity of post-tsynaptic neuron based on different values of γ, δ. By increasing δ and decreasing γ, the spiking activity of post-synaptic neuron is regulated. In this case, when the pre-synaptic neuron is already in the resting state, the post-synaptic neuron starts to activate again.

7. Discussion

As mentioned, the CNS is made of some basic building blocks: neurons, synapses, and astrocytes. Neurons, as a primary blocks in this biological network, can receive, process, and transmit data to other parts of system. In this context, synaptic coupling between two coupled neurons (pre-synaptic and post-synaptic neurons) can occur if the pre-synaptic neurons can trigger the synaptic gap by appropriate signaling. When this transmission is complete, post-synaptic neuron also starts to undergo spiking activity, with a rate proportional to its synaptic excitation, which is provided by the synaptic cleft. Indeed, after triggering the synapse by the pre-synaptic neurons, it makes an increase or decrease in the level of stimulus current for the post-synaptic neurons [88,98]. In this case event, the astrocyte module can act as a controller for regulating the neurons' activity. On the other hand, the astrocyte can control the applied stimulation current that is injected into the post-neuron. If the synaptic current to the post-neuron starts to increase strongly, by th proper selection of the astrocyte parameters, the additional spike trains will be removed

and some problems such as epilepsy can be controlled [77,82,88,99,100]. Consequently, by proper selection of the astrocyte parameters such as α, β, δ, and γ, the neuronal activity can be modulated and the biological system will be controlled.

The main purposes of different papers can now be compared. In [75], a digital realization of the neuron–astrocyte model with dynamic behaviors are presented in low-cost and high-speed approximation-based states. In [76], the digital realization of the Adex neuronal model on FPGA platforms is implemented. In [89], the behavior of a set of benchmark designs in VHDL–AMS and SystemC-AMS is modeled. In [88], a complete neuron–astrocyte digital implementation is proposed based on the low-error function approximation. In [83], a digital implementation of a biological astrocyte with Hopf oscillator interaction is considered. In [84], a reconfigurable and efficient 2-D neuron model capable of extending to higher dimensions is presented. In [85], just a digital implementation of astrocyte model is evaluated without any interactions with external forcing such as neurons. In [86,87], a digital implementation of neuron–astrocyte model is implemented without any consideration of the controlling effects of astrocyte on neurons, and the synaptic terminal model is different from the model we used. In this paper, a VHDL–AMS modeling of neuron–astrocyte is presented. In this approach, it is proved that by the proper selection of astrocyte coupling coefficients, the neurons' behavior can be controlled and the neuron–astrocyte communication mechanisms are modulated. In fact, this technique (behavioral modeling) brings down the simulation time of the design while having good accuracy and run time without any approximation for the non-linear systems.

8. Conclusions

This paper presents a modeling of neuron–astrocyte interaction using VHDL–AMS. In the general case, the effect of astrocytes on the neurons behavior is considered. The effect of astrocytes in three general states is analyzed; it was expected that neuronal activity is regulated by proper choice in the astrocyte parameters. Therefore, astrocyte cell has a very significant and vital role in the regulation of neuroglial interaction mechanisms, and if astrocytes do not work properly in the CNS, this can have a corrupting influence on the neurons' behavior.

Author Contributions: Conceptualization, M.A., F.B., E.N. and O.T.; Software, M.A., F.B., E.E.-Z. and O.T.; Writing—Review and Editing, M.A., A.R., E.E.-Z. and O.T.; Funding acquisition, M.A., O.T. and E.E.-Z. All authors have read and agreed to the published version of the manuscript.

Funding: We acknowledge the support by the German Research Foundation and the Open Access Publication Fund of the Thueringer Universitaets- und Landesbibliothek Jena Projekt-Nr. 433052568. The Deanship of Scientific Research (DSR) at King Abdulaziz University, Jeddah, Saudi Arabia has funded this project, under grant no. (FP-210-43).

Institutional Review Board Statement: Not applicable.

Informed Consent Statement: Not applicable.

Data Availability Statement: Data are contained within the article.

Conflicts of Interest: The authors declare no conflict of interest.

References

1. Roshani, G.; Nazemi, E.; Roshani, M. Usage of two transmitted detectors with optimized orientation in order to three phase flow metering. *Measurement* **2017**, *100*, 122–130. [CrossRef]
2. Hosseinzadeh-Bandbafha, H.; Nazemi, F.; Khounani, Z.; Ghanavati, H.; Shafiei, M.; Karimi, K.; Lam, S.S.; Aghbashlo, M.; Tabatabaei, M. Safflower-based biorefinery producing a broad spectrum of biofuels and biochemicals: A life cycle assessment perspective. *Sci. Total Environ.* **2021**, *802*, 149842. [CrossRef]
3. Roshani, G.; Nazemi, E.; Roshani, M. Intelligent recognition of gasoil-water three-phase flow regime and determination of volume fraction using radial basis function. *Flow Meas. Instrum.* **2017**, *54*, 39–45. [CrossRef]
4. Karami, A.; Yousefi, T.; Harsini, I.; Maleki, E.; Mahmoudinezhad, S. Neuro-Fuzzy Modeling of the Free Convection Heat Transfer from a Wavy Surface. *Heat Transf. Eng.* **2015**, *36*, 847–855. [CrossRef]

5. Alwan, S.; Al-Saeed, M.; Abid, H. Safety assessment and biochemical evaluation of biogenic silver nanoparticles (using bark extract of C. zeylanicum) in Rattus norvegicus rats. *Baghdad J. Biochem. Appl. Biol. Sci.* **2021**, *2*, 138–150. [CrossRef]
6. Nazemi, F.; Karimi, K.; Denayer, J.F.; Shafiei, M. Techno-economic aspects of different process approaches based on brown macroalgae feedstock: A step toward commercialization of seaweed-based biorefineries. *Algal. Res.* **2021**, *58*, 102366. [CrossRef]
7. Liu, Y.; Jiang, B.; Zhao, L.; Zhao, L.; Wang, Q.; Wang, C.; Xu, B. A dansyl-based fluorescent probe for sensing Cu2+ in aqueous solution. *Spectrochim. Acta Part A Mol. Biomol. Spectrosc.* **2021**, *261*, 120009. [CrossRef]
8. Roshani, M.; Sattari, M.A.; Ali, P.J.M.; Roshani, G.H.; Nazemi, B.; Corniani, E.; Nazemi, E. Application of GMDH neural network technique to improve measuring precision of a simplified photon attenuation based two-phase flowmeter. *Flow Meas. Instrum.* **2020**, *75*, 101804. [CrossRef]
9. Shalaby, M.N.; Sakoury, M.M.; Kholif, M.A.; Alsayed, N.I. The role of Amino Acids in improving immunity and growth factors of Volleyball players. *J. Adv. Pharm. Educ. Res.* **2020**, *10*, 141.
10. Roshani, S.; Roshani, S. Design of a high efficiency class-F power amplifier with large signal and small signal measurements. *Measurement* **2020**, *149*, 106991. [CrossRef]
11. Pourbemany, J.; Mirjalily, G.; Abouei, J.; Raouf, A.H.F. Load Balanced Ad-Hoc On-Demand Routing Basedon Weighted Mean Queue Length Metric. In Proceedings of the Electrical Engineering (ICEE), Iranian Conference on IEEE, Mashhad, Iran, 8–10 May 2018; pp. 470–475.
12. Pirasteh, A.; Roshani, S.; Roshani, S. A modified class-F power amplifier with miniaturized harmonic control circuit. *AEU Int. J. Electron. Commun.* **2018**, *97*, 202–209. [CrossRef]
13. Jamshidi, M.B.; Roshani, S.; Talla, J.; Roshani, S.; Peroutka, Z. Size reduction and performance improvement of a microstrip Wilkinson power divider using a hybrid design technique. *Sci. Rep.* **2021**, *11*, 7773. [CrossRef] [PubMed]
14. Zhang, L.; Wang, X.; Zhang, Z.; Cui, Y.; Ling, L.; Cai, G. An Adaptative Control Strategy for Interfacing Converter of Hybrid Microgrid Based on Improved Virtual Synchronous Generator. *IET Renew. Power Gener.* **2021**, *15*, 2674–2685. [CrossRef]
15. Jamshidi, M.B.; Siahkamari, H.; Roshani, S.; Roshani, S. A compact Gysel power divider design using U-shaped and T-shaped resonators with harmonics suppression. *Electromagnetics* **2019**, *39*, 491–504. [CrossRef]
16. Roshani, S.; Roshani, S.; Zarinitabar, A. A modified Wilkinson power divider with ultra harmonic suppression using open stubs and lowpass filters. *Analog. Integr. Circuits Signal Process* **2019**, *98*, 395–399. [CrossRef]
17. Roshani, S.; Roshani, S. Design of a very compact and sharp bandpass diplexer with bended lines for GSM and LTE applications. *AEU Int. J. Electron. Commun.* **2019**, *99*, 354–360. [CrossRef]
18. Roshani, S.; Roshani, S. A compact coupler design using meandered line compact microstrip resonant cell (MLCMRC) and bended lines. *Wirel. Netw.* **2021**, *27*, 677–684. [CrossRef]
19. Pirasteh, A.; Roshani, S.; Roshani, S. Compact microstrip lowpass filter with ultrasharp response using a square-loaded modified T-shaped resonator. *Turk. J. Electr. Eng. Comput. Sci.* **2018**, *26*, 1736–1746. [CrossRef]
20. Jha, A.K.; Ali, A.; Kumar, M.; Kumar, M.; Badhani, P.P.; Murthy, N.B.S.; Chandrakant, K. Outcome of routine histopathological examination of gallbladder specimen following elective laparoscopic cholecystectomy. *J. Carcinog.* **2021**, *20*, 19. [CrossRef]
21. Leman, M.A.; Claramita, M.; Rahayu, G.R. Predicting Factors on Modeling Health Behavior: A Systematic Review. *Am. J. Health Behav.* **2021**, *45*, 268. [CrossRef]
22. Anil, M.A.; Rebello, R.M.; Bhat, J.S. Speech-language profile of a child with fahrs disease: Case report of a rare neurodegenerative disorder. *J. Nat. Sci. Biol. Med.* **2020**, *11*, 206.
23. Ghanbari, B. On the modeling of the interaction between tumor growth and the immune system using some new fractional and fractional-fractal operators. *Adv. Differ. Equ.* **2020**, *2020*, 585. [CrossRef]
24. Zhao, H. Prediction and Evaluation of Athletes' Positive Emotions Based on Emotional Intelligence Theory. *Rev. Psicol. Deporte (J. Sport Psychol.)* **2021**, *30*, 38–52.
25. Ghanbari, B. Chaotic behaviors of the prevalence of an infectious disease in a prey and predator system using fractional derivatives. *Math. Methods Appl. Sci.* **2021**, *44*, 9998–10013. [CrossRef]
26. Nabishah, B.M.; Merican, Z.; Morat, P.B.; Alias, A.K.; Khalid, B.A. Effects of steroid hormones pretreatment on isoprenaline-induced cyclic adenosine 3',5'-monophosphate in rat lung. *Gen. Pharmacol.* **1990**, *21*, 935–938. [CrossRef]
27. Das, S.; Selvaraji, K.; Dutta, M.; Isa, M.Z.A.; Moorthy, T.N. A pilot study on glaucoma and depth variation, A factor that affect the accuracy of eyewitness identification. *Int. J. Med. Toxicol. Leg. Med.* **2018**, *21*, 239–242. [CrossRef]
28. Bahari, R.; Alwi, M.N.M.; Ahmad, M.R. Translation and validation of the Malay posttraumatic stress disorder checklist for DSM-5 (MPLC-5). *Malays. J. Med. Health Sci.* **2019**, *15* (Suppl. S1), 15–20.
29. Ghanbari, B. A new model for investigating the transmission of infectious diseases in a preypredator system using a nonsingular fractional derivative. *Math. Methods Appl. Sci.* **2021**, *44*, 9998–10013. [CrossRef]
30. Yang, L.W.; Fattepur, S.; Nilugal, K.C.; Asmani, F.; Yusuf, E.; Ghani, M.N.A.; Abdullah, I. Neuroprotection of abelmoschus esculentus l. against diabetic neuropathy. *Asian J. Pharm. Clin. Res.* **2018**, *11*, 28–31. [CrossRef]
31. Shalaby, M.N.; Sakoury, M.M.A.; Al-jameel, S.S.; Alghamdi, A. The Effect of Diving for Different Years on CD34+ Stem Cells and Some Physiological Variables for Commercial Divers. *Int. J. Hum. Mov. Sport. Sci.* **2021**, *9*, 1146–1156.
32. Shalaby, M.N. The Effect of Whey Protein (Natural Nanoparticle) on Muscle Strength, GH, IGF, T. Protein and body composition. *Int. J. Pharm. Res. Allied Sci.* **2018**, *7*, 126–132.

33. Shalaby, M.N.; Fadl, M.A. Relative Indicators and Predicative Ability of Some Biological Variables on Cardiac Neural Activity for Volleyball Players. *Syst. Rev. Pharm.* **2020**, *11*, 834–840.
34. Djilali, S.; Ghanbari, B. The influence of an infectious disease on a prey-predator model equipped with a fractional-order derivative. *Adv. Differ. Equ.* **2021**, *2021*, 20. [CrossRef]
35. Roshani, G.H.; Nazemi, E.; Feghhi, S.A.H.; Setayeshi, S. Flow regime identification and void fraction prediction in two-phase flows based on gamma ray attenuation. *Measurement* **2015**, *62*, 25–32. [CrossRef]
36. Abolhasani, M.; Karami, A.; Rahimi, M. Numerical Modeling and Optimization of the Enhancement of the Cooling Rate in Concentric Tubes Under Ultrasound Field. *Numer. Heat Transf. Part A Appl.* **2015**, *67*, 1282–1309. [CrossRef]
37. Roshani, G.H.; Feghhi, S.A.H.; Mahmoudi-Aznaveh, A.; Nazemi, E.; Adineh-Vand, A. Precise volume fraction prediction in oil–water–gas multiphase flows by means of gamma-ray attenuation and artificial neural networks using one detector. *Measurement* **2014**, *51*, 34–41. [CrossRef]
38. Aghakhani, M.; Ghaderi, M.R.; Karami, A.; Derakhshan, A.A. Combined effect of TiO_2 nanoparticles and input welding parameters on the weld bead penetration in submerged arc welding process using fuzzy logic. *Int. J. Adv. Manuf. Technol* **2014**, *70*, 63–72. [CrossRef]
39. Nazemi, E.; Roshani, G.H.; Feghhi, S.A.H.; Setayeshi, S.; Zadeh, E.E.; Fatehi, A. Optimization of a method for identifying the flow regime and measuring void fraction in a broad beam gamma-ray attenuation technique. *Int. J. Hydrogen Energy* **2016**, *41*, 7438–7444. [CrossRef]
40. Karami, A.; Veysi, F.; Mohebbi, S.; Ghashghaei, D. Optimization of Laminar Free Convection in a Horizontal Cavity Consisting of Flow Diverters Using ICA. *Arab. J. Sci. Eng* **2014**, *39*, 2295–2306. [CrossRef]
41. Nazemi, E.; Feghhi, S.A.H.; Roshani, G.H.; Setayeshi, S.; Peyvandi, R.G. A radiation-based hydrocarbon two-phase flow meter for estimating of phase fraction independent of liquid phase density in stratified regime. *Flow Meas. Instrum.* **2015**, *46*, 25–32. [CrossRef]
42. Jiang, B.; Liu, Y.; Zhao, L.; Zhao, L.; Wang, C.; Liu, C.; Xu, B. Construction of a pH-sensitive self-assembly in aqueous solutions based on a dansyl-modified cyclodextrin. *Soft Matter* **2021**, *17*, 7516–7523. [CrossRef]
43. Nazemi, E.; Feghhi, S.A.H.; Roshani, G.H.; Peyvandi, R.G.; Setayeshi, S. Precise void fraction measurement in two-phase flows independent of the flow regime using gamma-ray attenuation. *Nucl. Eng. Technol.* **2016**, *48*, 64–71. [CrossRef]
44. Roshani, G.H.; Nazemi, E.; Feghhi, S.A.H. Investigation of using 60Co source and one detector for determining the flow regime and void fraction in gas–liquid two-phase flows. *Flow Meas. Instrum.* **2016**, *50*, 73–79. [CrossRef]
45. Sattari, M.A.; Roshani, G.H.; Hanus, R.; Nazemi, E. Applicability of time-domain feature extraction methods and artificial intelligence in two-phase flow meters based on gamma-ray absorption technique. *Measurement* **2021**, *168*, 108474. [CrossRef]
46. Basahel, A.; Sattari, M.; Taylan, O.; Nazemi, E. Application of Feature Extraction and Artificial Intelligence Techniques for Increasing the Accuracy of X-ray Radiation Based Two Phase Flow Meter. *Mathematics* **2021**, *9*, 1227. [CrossRef]
47. Moradi, M.J.; Hariri-Ardebili, M.A. Developing a Library of Shear Walls Database and the Neural Network Based Predictive Meta Model. *Appl. Sci.* **2019**, *9*, 2562. [CrossRef]
48. Nazemi, B.; Rafiean, M. Forecasting house prices in Iran using GMDH. *Int. J. Hous. Mark. Anal.* **2021**, *14*, 555–568. [CrossRef]
49. Moradi, M.J.; Roshani, M.M.; Shabani, A.; Kioumarsi, M. Prediction of the Load-Bearing Behavior of SPSW with Rectangular Opening by RBF Network. *Appl. Sci.* **2020**, *10*, 1185. [CrossRef]
50. Moradi, M.; Daneshvar, K.; Ghazi-Nader, D.; Hajiloo, H. The prediction of fire performance of concrete-filled steel tubes (CFST) using artificial neural network. *Thin Walled Struct.* **2021**, *161*, 107499. [CrossRef]
51. Zajmi, L.; Ahmed, F.Y.; Jaharadak, A.A. Concepts, methods, and performances of particle swarm optimization, backpropagation, and neural networks. *Appl. Comput. Intell. Soft Comput.* **2018**, *2018*, 9547212. [CrossRef]
52. Amidi, Y.; Nazari, B.; Sadri, S.; Yousefi, A. Parameter Estimation in Multiple Dynamic Synaptic Coupling Model Using Bayesian Point Process State-Space Modeling Framework. *Neural Comput.* **2021**, *33*, 1269–1299. [CrossRef]
53. Yousefi, A.; Amidi, Y.; Nazari, B.; Eden, U.T. Assessing Goodness-of-Fit in Marked Point Process Models of Neural Population Coding via Time and Rate Rescaling. *Neural Comput.* **2020**, *32*, 2145–2186. [CrossRef] [PubMed]
54. Roshani, M.; Phan, G.; Roshani, G.H.; Hanus, R.; Nazemi, B.; Corniani, E.; Nazemi, E. Combination of X-ray tube and GMDH neural network as a nondestructive and potential technique for measuring characteristics of gas-oil–water three phase flows. *Measurement* **2021**, *168*, 108427. [CrossRef]
55. Roshani, M.; Phan, G.; Faraj, R.H.; Phan, N.H.; Roshani, G.H.; Nazemi, B.; Corniani, E.; Nazemi, E. Proposing a gamma radiation based intelligent system for simultaneous analyzing and detecting type and amount of petroleum by-products. *Nucl. Eng. Technol.* **2021**, *53*, 1277–1283. [CrossRef]
56. Roshani, G.; Nazemi, E. Intelligent densitometry of petroleum products in stratified regime of two phase flows using gamma ray and neural network. *Flow Meas. Instrum.* **2017**, *58*, 6–11. [CrossRef]
57. Karami, A.; Roshani, G.H.; Khazaei, A.; Nazemi, E.; Fallahi, M. Investigation of different sources in order to optimize the nuclear metering system of gas–oil–water annular flows. *Neural Comput. Appl.* **2020**, *32*, 3619–3631. [CrossRef]
58. Karami, A.; Roshani, G.H.; Nazemi, E.; Roshani, S. Enhancing the performance of a dual-energy gamma ray based three-phase flow meter with the help of grey wolf optimization algorithm. *Flow Meas. Instrum.* **2018**, *64*, 164–172. [CrossRef]
59. Roshani, G.H.; Roshani, S.; Nazemi, E.; Roshani, S. Online measuring density of oil products in annular regime of gas-liquid two phase flows. *Measurement* **2018**, *129*, 296–301. [CrossRef]

60. Alkabaa, A.S.; Nazemi, E.; Taylan, O.; Kalmoun, E.M. Application of Artificial Intelligence and Gamma Attenuation Tech-niques for Predicting Gas–Oil–Water Volume Fraction in Annular Regime of Three-Phase Flow Independent of Oil Pipeline's Scale Layer. *Mathematics* **2021**, *9*, 1460. [CrossRef]
61. Roshani, G.; Nazemi, E.; Roshani, M. Identification of flow regime and estimation of volume fraction independent of liquid phase density in gas-liquid two-phase flow. *Prog. Nucl. Energy* **2017**, *98*, 29–37. [CrossRef]
62. Roshani, G.; Hanus, R.; Khazaei, A.; Zych, M.; Nazemi, E.; Mosorov, V. Density and velocity determination for single-phase flow based on radiotracer technique and neural networks. *Flow Meas. Instrum.* **2018**, *61*, 9–14. [CrossRef]
63. Djilali, S.; Ghanbari, B. Dynamical behavior of two predators-one prey model with generalized functional response and time-fractional derivative. *Adv. Differ. Equ.* **2021**, *2021*, 235. [CrossRef]
64. Ghanbari, B. Abundant exact solutions to a generalized nonlinear Schrödinger equation with local fractional derivative. *Math. Methods Appl. Sci.* **2021**, *44*, 8759–8774. [CrossRef]
65. Ghanbari, B. On novel nondifferentiable exact solutions to local fractional Gardner's equation using an effective technique. *Math. Methods Appl. Sci.* **2021**, *44*, 4673–4685. [CrossRef]
66. Nabti, A.; Ghanbari, B. Global stability analysis of a fractional SVEIR epidemic model. *Math. Methods Appl. Sci.* **2021**, *44*, 8577–8597. [CrossRef]
67. Ghanbari, B. On approximate solutions for a fractional prey-predator model involving the Atangana-Baleanu derivative. *Adv. Differ. Equ.* **2020**, *2020*, 679. [CrossRef]
68. Ghanbari, B. A fractional system of delay differential equation with nonsingular kernels in modeling hand-foot-mouth disease. *Adv. Differ. Equ.* **2020**, *2020*, 536. [CrossRef]
69. Ghanbari, B.; Atangana, A. Some new edge detecting techniques based on fractional derivatives with non-local and non-singular kernels. *Adv. Differ. Equ.* **2020**, *2020*, 435. [CrossRef]
70. Ghanbari, B.; Nisar, K.S.; Aldhaifallah, M. Abundant solitary wave solutions to an extended nonlinear Schrödinger's equation with conformable derivative using an efficient integration method. *Adv. Differ. Equ.* **2020**, *2020*, 328. [CrossRef]
71. Ghanbari, B.; Yusuf, A.; Baleanu, D. The new exact solitary wave solutions and stability analysis for the $(2+1)$-dimensional Zakharov-Kuznetsov equation. *Adv. Differ. Equ.* **2019**, *2019*, 49. [CrossRef]
72. Srivastava, H.M.; Günerhan, H.; Ghanbari, B. Exact traveling wave solutions for resonance nonlinear Schrödinger equation with intermodal dispersions and the Kerr law nonlinearity. *Math. Methods Appl. Sci.* **2019**, *42*, 7210–7221. [CrossRef]
73. Ghanbari, B.; Rada, L. Solitary wave solutions to the Tzitzeica type equations obtained by a new efficient approach. *J. Appl. Anal. Comput.* **2019**, *9*, 568–589. [CrossRef]
74. Rahman, G.; Nisar, K.S.; Ghanbari, B.; Abdeljawad, T. On generalized fractional integral inequalities for the monotone weighted Chebyshev functionals. *Adv. Differ. Equ.* **2020**, *2020*, 368. [CrossRef]
75. Haghiri, S.; Ahmadi, A.; Saif, M. VLSI implementable neuron-astrocyte control mechanism. *Neurocomputing* **2016**, *214*, 280–296. [CrossRef]
76. Gomar, S.; Ahmadi, A. Digital multiplierless implementation of biological adaptive-exponential neuron model. *IEEE Trans. Circuits Syst. I* **2013**, *61*, 1206–1219. [CrossRef]
77. Postnov, D.E.; Ryazanov, L.S.; Sosnovtsev, O.V. Functional modeling of neural-glial interaction. *BioSystems* **2007**, *89*, 8491. [CrossRef]
78. Araque, A.; Parpura, V.; Sanzgiri, R.P.; Haydon, P.G. Tripartite synapses: Glia, the unacknowledged partner. *Trends Neurosci.* **1999**, *22*, 208–215. [CrossRef]
79. Volman, V.; Ben-Jacob, E.; Levine, H. The astrocyte as a gatekeeper of synaptic information transfer. *Neural Comput.* **2007**, *19*, 303–326. [CrossRef]
80. Valenza, G.; Pioggia, G.; Armato, A.; Ferro, M.; Scilingo, E.P.; de Rossi, D. A neuron–astrocyte transistor-like model for neuromorphic dressed neurons. *Neural Netw.* **2011**, *24*, 679–685. [CrossRef]
81. Ghaderi, V.S.; Allam, S.L.; Ambert, N.; Bouteiller, J.-C.; Choma, J. Modeling Neuron-Glia Interactions: From Parametric Model to Neuromorphic Hardware. In Proceedings of the 33rd Annual International Conference of the IEEE EMBS, Boston, MA, USA, 30 August–3 September 2011.
82. Postnov, D.E.; Koreshkov, R.N.; Brazhe, N.A.; Brazhe, A.R.; Sosnovtseva, O.V. Dynamical patterns of calcium signaling in a functional model of neuron–astrocyte networks. *J. Biol. Phys.* **2009**, *35*, 425–445. [CrossRef] [PubMed]
83. Soleimani, H.; Bavandpour, M.; Ahmadi, A.; Abbott, D. Digital implementation of a biological astrocyte model and its application. *IEEE Trans. Neural Netw.* **2014**, *26*, 127–139. [CrossRef] [PubMed]
84. Soleimani, H.; Drakakis, E.M. An efficient and reconfigurable synchronous neuron model. *IEEE Trans. Circuits Syst. II* **2017**, *6*, 91–95. [CrossRef]
85. Nazari, S.; Faez, K.; Karimi, E.; Amiri, M. A digital neurmorphic circuit for a simplified model of astrocyte dynamics. *Neurosci. Lett.* **2014**, *582*, 21–26. [CrossRef]
86. Nazari, S.; Amiri, M.; Faez, K.; Amiri, M. Multiplierless digital implementation of neuron–astrocyte signalling on FPGA. *Neurocomputing* **2015**, *164*, 281–292. [CrossRef]
87. Nazari, S.; Faez, K.; Amiri, M.; Karimi, E. A digital implementation of neuron–astrocyte interaction for neuromorphic applications. *Neural Netw.* **2015**, *66*, 79–90. [CrossRef] [PubMed]

88. Haghiri, S.; Ahmadi, A.; Saif, M. Complete Neuron-Astrocyte Interaction Model: Digital Multiplierless Design and Networking Mechanism. *IEEE Trans. Biomed. Circuits Syst.* **2017**, *11*, 117–127. [CrossRef] [PubMed]
89. Narayanan, R.; Abbasi, N.; Al Sammane, G.; Zaki, M.; Tahar, S. A Comparative Study of AMS Circuit Simulation in VHDL-AMS and SystemC-AMS. In Proceedings of the IEEE International Conference on Embedded Systems and Critical Applications, Tunis, Tunisia, 15–16 May 2008; Volume 5, pp. 23–28.
90. Ashenden, P.J.; Peterson, G.D.; Teegarden, D.A. *The System Designer's Guide to VHDL-AMS*; Morgan Kaufmann: San Francisco, CA, USA, 2002.
91. de Pitta, M.; Volman, V.; Levine, G.; Pioggia, D.; de Rossi, D.; Ben-Jacob, E. Coexistence of amplitude and frequency modulations in intracellular calcium dynamics. *Phys. Rev. E* **2008**, *77*, 030903. [CrossRef] [PubMed]
92. Nadkarni, S.; Jung, P. Dressed neurons: Modeling neural-glia interactions. *Phys. Biol.* **2004**, *1*, 35–41. [CrossRef] [PubMed]
93. Parpura, V.; Haydon, P. Physiological astrocytic calcium levels stimulate glutamate release to modulate adjacent neurons. *Proc. Natl. Acad. Sci. USA* **2000**, *97*, 8629–8634. [CrossRef]
94. Izhikevich, E.M. Dynamical Systems in Neuroscience: The Geometry of Excitability and Bursting. In *Computational Neuroscience*; MIT Press: Cambridge, MA, USA, 2006.
95. Kopell, N.; Ermentrout, G.B.; Whittington, M.A.; Traub, R.D. Gamma rhythms and beta rhythms have different synchronization properties. *Proc. Natl. Acad. Sci. USA* **2000**, *97*, 1867–1872. [CrossRef]
96. Zobeiri, M.; Luijtelaar, G.V.; Budde, T.; Sysoev, I.V. The Brain Network in a Model of Thalamocortical Dysrhythmia. *Brain Connect.* **2019**, *9*, 273–284. [CrossRef] [PubMed]
97. Medvedeva, T.M.; Sysoeva, M.V.; van Luijtelaar, G.; Sysoev, I.V. Modeling spike-wave discharges by a complex network of neuronal oscillators. *Neural Netw.* **2018**, *98*, 271–282. [CrossRef] [PubMed]
98. Vich, C.; Prohens, R.; Teruel, A.E.; Guillamon, A. Estimation of Synaptic Activity during Neuronal Oscillations. *Mathematics* **2020**, *8*, 2153. [CrossRef]
99. Orcioni, S.; Paffi, A.; Apollonio, F.; Liberti, M. Revealing Spectrum Features of Stochastic Neuron Spike Trains. *Mathematics* **2020**, *8*, 1011. [CrossRef]
100. Ascione, G.; Toaldo, B. A Semi-Markov Leaky Integrate-and-Fire Model. *Mathematics* **2019**, *7*, 1022. [CrossRef]